ARTICLE

Robust All-Carbon Molecular Junctions on Flexible or Semi-Transparent Substrates Using "Process-Friendly" Fabrication

Amin Morteza Najarian,[†,‡] Bryan Szeto,[‡] Ushula M. Tefashe,[†,‡] and Richard L. McCreery[*,†,‡]

[†]Department of Chemistry, University of Alberta, Edmonton, Alberta T6G 2R3, Canada
[‡]National Institute for Nanotechnology, National Research Council Canada, Edmonton, Alberta T6G 2G2, Canada

Ⓢ *Supporting Information*

ABSTRACT: Large area molecular junctions were fabricated on electron-beam deposited carbon (eC) surfaces with molecular layers in the range of 2–5.5 nm between conducting, amorphous carbon contacts. Incorporating eC as an interconnect between Au and the molecular layer improves substrate roughness, prevents electromigration and uses well-known electrochemistry to form a covalent C—C bond to the molecular layer. Au/eC/anthraquinone/eC/Au junctions were fabricated on Si/SiO$_x$ with high yield and reproducibility and were unchanged by 10^7 current–voltage cycles and temperatures between 80 and 450 K. Au/eC/AQ/eC/Au devices fabricated on plastic films were unchanged by 10^7 current density vs bias voltage (J–V) cycles and repeated bending of the entire assembled junction. The low sheet resistance of Au/eC substrates permitted junctions with sufficiently transparent electrodes to conduct Raman or UV–vis absorption spectroscopy in either reflection or transmission geometries. Lithographic patterning of Au/eC substrates permitted wafer-scale integration yielding 500 devices on 20 chips on a 100 mm diameter wafer. Collectively, eC on Au provides a platform for fabrication and operation of chemically stable, optically and electrically functional molecules on rigid or flexible materials. The relative ease of processing and the robustness of molecular junctions incorporating eC layers should help address the challenge of economic fabrication of practical, flexible molecular junctions for a potentially wide range of applications.
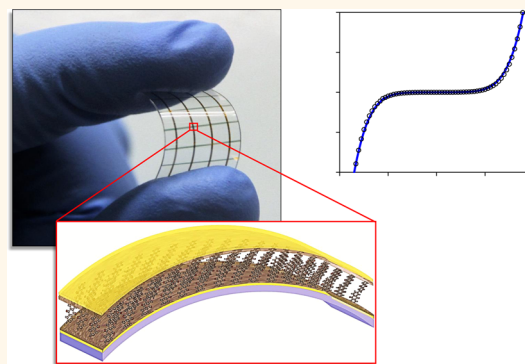
KEYWORDS: *flexible electronics, molecular junction, amorphous carbon, optical transparency, flexible carbon films, photolithography*

Development of the field of Molecular Electronics was stimulated by intense scientific interest in the behavior of single molecules or molecular monolayers as elements in electronic circuits. The small size and wide range of electronic configurations of molecules were investigated to enable new electronic functions and possibly further extend the exponential increase in device density in microelectronic devices. Recent reviews of the progress of molecular electronics document the many experimental paradigms used to provide contact between conventional conductors and molecular components,[1−3] notably the quest for a molecular rectifier first proposed in 1974.[4] The current report deals with "ensemble" molecular junctions (MJs), in which a large number of molecules are bonded to a conductive substrate, then a "top contact" is applied by one of several methods. Many distinct electronic effects of ensemble molecular devices have been demonstrated, such as nonlinearity,[5−8] rectification,[9−13] bist-ability,[14,15] photocurrents,[13,16−19] light emission,[20−22] and redox events.[15,23−25] A key issue of molecular electronics is

integration of molecular devices into microelectronic circuits, with sufficient lifetime and temperature tolerance to be widely practical in real applications. The impediments to developing robust, practical MJs often lie in the requirement for substrates which are flat on a molecular scale, possible electromigration or oxidation of metallic contacts, and the difficulties in adapting laboratory fabrication methods to real-world processing and operating conditions.

Our group has developed carbon-based molecular junctions based on covalent bonding of molecular layers to flat (<0.4 nm rms) sp^2 hybridized carbon surfaces made by pyrolysis of novolac photoresist, that is, pyrolyzed photoresist films (PPF). PPF is patternable by photolithography, thermally stable, not subject to electromigration, and electrochemical reduction of diazonium reagents on PPF provides a variety of molecular
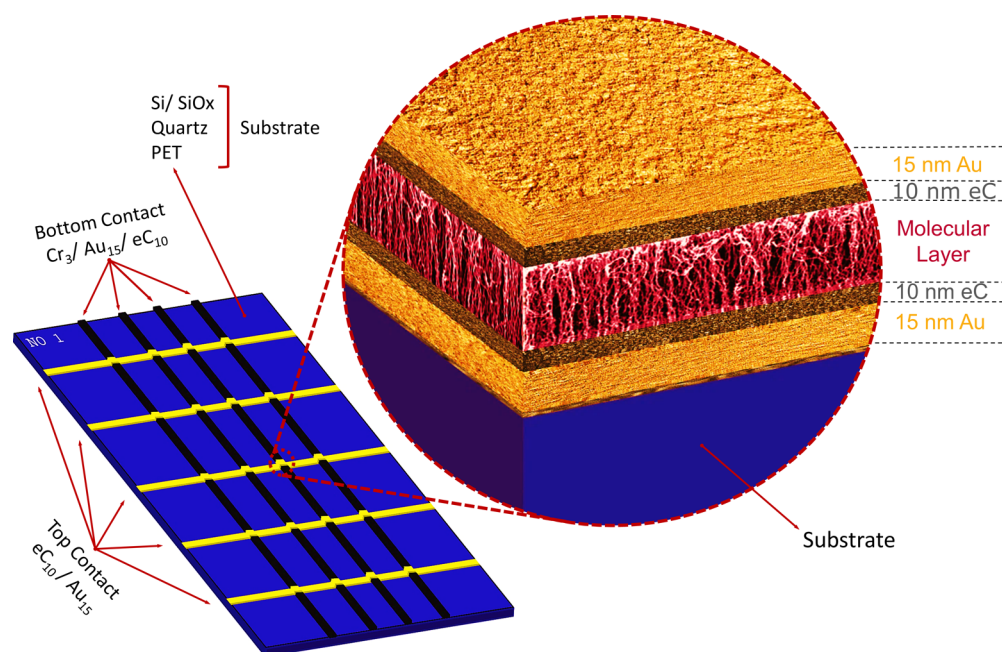
Figure 1. Schematic illustrations Au/eC/molecule/eC/Au molecular junctions suing electron-beam deposited carbon adjacent to molecular layer. Each chip is 1.8 × 1.2 cm. Final dimension of each junction is 250 × 250 μm.
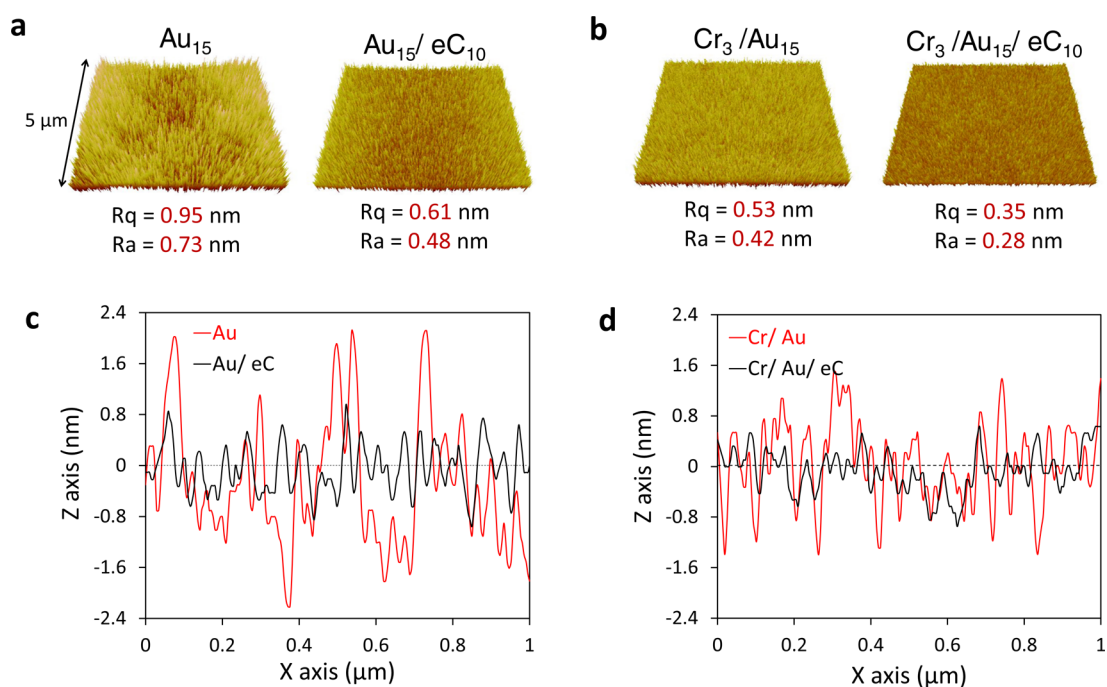
Figure 2. (a) AFM images of e-beam deposited Au and Au/eC surfaces on Si/SiO$_x$ substrate. Subscripts indicate thicknesses of each deposited layer in nanometers. Ra and Rq are average and root-mean-square roughness, respectively. (b) AFM images of the surface of e-beam deposited Cr/Au and Cr/Au/eC surfaces on Si/SiO$_x$ substrate. (c) AFM line scan profiles of surfaces shown in panel (a). (d) AFM line scan profiles of surfaces shown in panel (b).

layer structures and thicknesses. A top contact of electron beam deposited carbon (eC) or Cu yields molecular junctions with high yield (>90%), good reproducibility, long cycle life (>10^9 scans)[26] and wide temperature tolerance (6−600 K).[26,27] PPF/ azobenzene/eC/Au MJs were produced for implementation in audio processing, and consumer devices containing 390 MJs were sold publically in late 2015.[28]

PPF is structurally similar to glassy carbon, but is a relatively poor conductor (∼200 S/cm), and the requirement for slow

pyrolysis at >1000 °C in forming gas is not readily amenable to large scale manufacturing. PPF can be made thin enough to provide partial optical transparency,[29,30] but its low conductivity as a thin film restricts possible applications. The current research was undertaken to combine the high conductivity and partial transparency of thin metal films with the flatness and surface modification chemistry of PPF while also avoiding high temperature processing. Electron-beam deposited carbon has been described previously for deposition

of 7–300 nm thick films of conducting carbon on quartz[31,32] or silicon,[33] in some cases resulting in a partially transparent electrode. We describe below an "all-carbon" molecular junction consisting of a covalently bonded molecular layer between Au/carbon electrodes made by successive electron-beam deposition of Au and carbon at room temperature shown schematically in Figure 1. Complete molecular junctions may be fabricated on rigid or flexible materials and retain the strong C–C bond which underlies the stability of diazonium-derived molecular layers. The resulting carbon/molecule/carbon MJs can be made with conventional vacuum deposition with high yield and excellent stability while avoiding the high temperatures and material transfer steps often required for previous MJ designs.

RESULTS AND DISCUSSION

E-Beam Carbon Properties. As the feature size of the active component decreases, factors such as electromigration, surface roughness, film uniformity and stability of electrodes begin to limit device performance.[34−36] Experience with numerous MJs having molecular layers of 1–5 nm thickness indicates that substrate roughness should be less than 0.5 nm rms (by AFM); for example, the PPF used in previous reports[5,6,26,37,38] and in commercial devices[28] ranged from 0.4 to 0.5 nm rms. Figure 2 shows AFM images and line scans of various films deposited on Si/SiO_x(300 nm) with an initial roughness of 0.15 nm rms. E-beam deposition of Au directly onto Si/SiO_x forms the well-known island film with high rms roughness (R_q) of 0.95 nm and peak-to-peak variation (R_{pp}) often exceeding ±4 nm. Deposition of 10 nm of eC on top of this rough Au surface results in the smoother surface of Figure 2a, with R_q = 0.61 nm and R_{pp} of approximately ±1.5 nm. The decrease in roughness was unexpected because the low likelihood of carbon diffusion and island formation should track the underlying surface. The commonly used technique of applying a chromium adhesion layer to reduce roughness is shown in Figure 2b, with the resulting Cr_3/Au_{15} film having R_q = 0.53 nm and R_{pp} of ±2.5 nm. eC deposition on this surface also reduces roughness (Figure 2d) to R_q = 0.35 nm and R_{pp} of ±1.5 nm. [Note that subscripts on layer identities indicate layer thickness in nm, e.g., Au_{15}.] The roughness decrease is very consistent, and valuable for subsequent fabrication of MJs, with one possible origin of the effect being rapid formation of covalent bonds between incoming carbon atoms and clusters forming a "superlayer" which bridges defects or grain boundaries in the underlying metal.

The resistivity of PPF is in the range of 0.003 to 0.006 Ω·cm for pyrolysis at 1100 °C, although this value varies significantly with film thickness and thermal history.[37,39−41] It is similar to the 0.005 Ω·cm reported for glassy carbon, consistent with a glassy, sp^2 carbon material. An early report on eC deposited on quartz reported a sheet resistance of 2000−5000 Ω/square for a 300 nm film, corresponding to a resistivity of 0.06 to 0.15 Ω·cm.[31] Four-point probe measurements were carried out on eC films deposited directly on quartz yield the results shown in Table 1, which are averages of five measurements across a "blanket" eC film for each thickness. eC films that are 10 to 30 nm thick have sheet resistances of $10^4−10^5$ Ω/□, yielding resistivities of 0.03 to 0.16 Ω·cm, similar to that reported for the 300 nm thick film.[31] The low conductivity of eC can result in significant ohmic losses in thin films, with a 10 nm film of a 0.05 × 1 cm strip having a predicted resistance of ~3 MΩ. However, we showed previously that because the current in a

Table 1. Four-Point Probe Resistances of eC and Au Films on Quartz, Q, and SiOₓ

	sheet resistance (Ω/□)	resistivity (Ω·cm)
$Q/eC_{3(a)}$	1.04×10^9	312
Q/eC_{10}	167400	0.167
Q/eC_{20}	19940	0.040
Q/eC_{30}	11310	0.034
mean (10−30 nm)		0.080
$Q/Cr_4/Au_{15}/eC_{10}$	2.98	
$Q/Cr_4/Au_{30}/eC_{10}$	1.03	
$Si/SiO_x/Cr_4/Au_{30}/eC_{10}$	1.05	
PPF (1000 nm)[39]	51	0.005
eC (310 nm)[31]	44000	0.136
OTPPF[b](40 nm)[29]	500	0.002

[a]Subscripts denote layer thicknesses in nm. [b]Optically transparent PPF.

MJ passes through the short dimension of the eC film (i.e., 10 nm), its contribution to resistance is negligible, and the current density vs bias voltage (J–V) responses of PPF/NAB/eC/Au MJs were indistinguishable for eC thicknesses of 2 to 30 nm (NAB = nitroazobenzene).[38] In order to use eC as a substrate, it was deposited onto a Cr_3/Au_{15} film, without breaking vacuum. The sheet resistances of various Au/eC bilayers listed in Table 1 are 1−3 Ω/□, compared to >10^4 Ω/□ for eC alone, reducing the resistance predicted for a 0.05 × 1 cm strip from 3 MΩ for eC_{10} alone to 60 Ω for a Au_{15}/eC_{10} bilayer. The Au carries most of the current in the lateral directions of the Au/eC film, and the eC_{10} resistance in series with the molecular layer is less than 0.3 mΩ for a 250 × 250 μm molecular junction. The higher conductivity of Au/eC films compared to PPF eliminates most of the ohmic potential error when acquiring J–V curves in two-wire mode, as shown in Supporting Information section 4.1. In addition, we will show below that the $Cr_3/Au_{15}/eC_{10}$ films are excellent substrates for molecular junction fabrication, are partially optically transparent, and can be patterned lithographically.

Raman spectra of e-beam carbon on silicon have been presented previously,[33] and show a broad peak from ~1000 to ~1600 cm^{-1} in the region of the sp^2 carbon bands, indicating a very disordered structure. Pyrolysis at 1000 °C led to observable "D" and "G" bands at ~1360 cm^{-1} and ~1600 cm^{-1}, similar in position to the bands observed for PPF. A more detailed Raman analysis was carried out for the current eC films in order to estimate the relative content of sp^2 and sp^3 bonded carbon as shown in Supporting Information section 3.1. Raman spectra of eC and PPF are compared in Figures S5 and S6, along with that of eC after annealing in forming gas at 1000 °C for 3 h. Several reports have described the deconvolution of the broad carbon bands into D and G components, and the relationship of their positions and intensities to the sp^3/sp^2 ratio of the carbon film.[42,43] Similar analysis and the resulting sp^3 contents are shown in Supporting Information Figures S4−S7. The as-deposited eC is estimated to be 30−40% sp^3 hybridized carbon, with the remainder sp^2, but the sp^3 content becomes negligible after annealing at 1000 °C (Figure S5). The same analysis applied to PPF and glassy carbon yields negligible sp^3 content (Figure S6 and S7). X-ray photoelectron spectroscopy (XPS) has also been used to estimate the sp^3/ sp^2 content of disordered carbon materials based on relative intensities of components of the C_{1s} band.[44,45] XPS spectra of the C_{1s} region for eC is shown in Figure S8, and the sp^3 content

indicated by the XPS is 30% for as-deposited eC, which decreases to 11% upon annealing (Figure S9). Although the sp^3 percentages from XPS and Raman should be considered approximate, they clearly indicate significant sp^3 content in as-deposited eC, which is distinct from that of PPF or annealed eC. The eC resembles various "diamond like carbon" materials[46−50] and sputtered carbon films[51,52] in this respect, although the microstructure and specific bonding geometries may be different. Note that eC is near the disordered extreme for carbon materials compared to fullerenes, diamond, and graphite and is likely isotropic in its structure and properties. The important properties of eC for MJ fabrication are flatness, sufficient conductivity, stability, substrate adhesion, ability to modify the eC surface with covalent C−C bonds to molecular layers, and suitability for lithographic patterning, as described below.

Voltammetric curves for reduction of 2-anthraquinone (AQ) diazonium reagent are compared in Figure 3 for PPF, Au, and
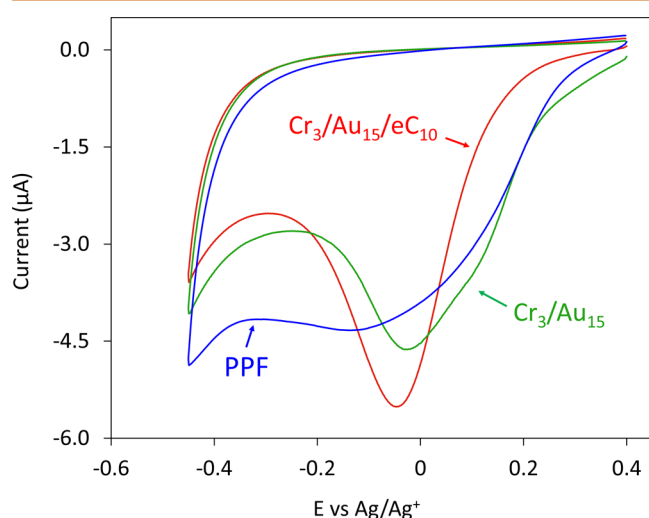
Figure 3. Cyclic voltammograms of Anthraquinone diazonium solution on PPF, Cr/Au, and Cr/Au/eC surfaces. The solution was contained 1 mM AQ diazonium fluoroborate in acetonitrile with 0.1 M tetrabutylammonium hexafluorophosphate (TBAPF$_6$) as supporting electrolyte, and scan rate was 50 mV/s for all cases. Detailed grafting conditions and cyclic voltammograms are shown in Supporting Information section 2.2.

eC, in acetonitrile in all cases. The reduction peak corresponds to formation of a phenyl radical which binds to the surface as a mono- or multilayer. The shape and peak potential of the reduction wave on PPF vary for different diazonium precursors, but in all cases studied to date, the reduction peaks are better defined on Au/eC than on PPF. The lower resistance of the Au/eC contact avoids ohmic potential error, and the greater structural disorder of eC likely has more nucleation sites for phenyl radical attachment. As will be described next, well-defined electrochemical layer formation also contributes to high junction reliability.

Electronic Behavior of eC/Molecule/eC Junctions. Current density vs bias voltage ($J−V$) curves for five thicknesses of AQ in Si/SiO$_x$/Cr$_3$/Au$_{15}$/eC$_{10}$/AQ$_x$/eC$_{10}$/Au$_{15}$ molecular junctions are shown in Figure 4, on both linear (panel a) and semilogarithmic scales (panel b). The yield (number of MJs not shorted) for all junctions fabricated with eC is 100% and the standard deviations of current density are

shown in Figure 4 as error bars and also are listed in Table S4. Vapor-deposited Au has been used successfully for ensemble MJ fabrication,[11,12,53] but in most cases requires template stripping to provide a sufficiently flat substrate surface.[8,9,54−59] Figure 4c shows results from junctions fabricated with an identical procedure to that for Figure 4a, but omitting the substrate eC layer to yield Cr$_3$/Au$_{15}$/AQ$_x$/eC$_{10}$/Au$_{15}$. For the e-beam deposited Au substrate without the additional eC layer, the yield was low (>50% "shorts") and reproducibility of nonshorted devices was poor. The variability of current density was large enough to obscure the effect of AQ thickness, as evident from comparison of the 3 and 5.3 nm cases. A more complete test of the effect of thickness on $J−V$ behavior is shown in Figure 4d, which plots ln(J) at $V = 0.1$ V vs AQ layer thickness for three different substrates. The slope of such plots yields the attenuation coefficient β, which is widely used to compare the thickness dependences of molecular tunnel junctions.[3,60−62] The slope and intercept of the β plot for PPF (Figure 4d) are −2.8 ± 0.13 and 4.7 ± 0.55, respectively. The slope and intercept of the same plot for Au/eC are −2.7 ± 0.12 and 4.7 ± 0.47. These results from PPF and Au/eC electrodes are statistically indistinguishable, and comparable to the −2.7 ± 0.6 nm^{-1} slope observed for eight aromatic MJs in PPF/molecule/Cu devices.[6] J values for the Au substrate lacking the eC$_{10}$ layer deviated greatly from the line in Figure 4d and exhibited the high standard deviations apparent in Figure 4c.

One advantage of "all carbon" MJs is stability, with the eC layers resistant to both oxidation and electromigration. We reported previously that PPF/nitroazobenzene/eC/Au were unchanged by current densities exceeding 1000 A/cm^2 at ±3 V, whereas the analogous PPF/nitroazobenzene/Cu/Au broke down when the Cu/Au was biased more positive than +2 V.[38] The present Au/eC/AQ/eC/Au devices were subjected to several stability tests, with the results shown in Figure 5. Panel a shows a typical $J−V$ response for a MJ with a 3.4 nm layer of AQ, both initially and after storage in air for 85 days. Figure 5b shows a different device before and after scanning 10^7 times to ±1.3 V in air and shows no changes in shape or current magnitude. This high operational stability significantly exceeds that using different self-assembly fabrication methods reported in the literature.[63−67] Figure 5c shows $J−V$ responses acquired between 80 and 450 K in vacuum, and the associated Arrhenius plot is provided in Supporting Information Figure S12. The apparent activation energies are similar to those observed for PPF/molecule/Cu MJs,[26] with near zero slope between 77 and 150 K and ∼38 meV slope near 300 K. As noted above, the successful application of 390 PPF/azobenzene/eC/Au devices in consumer electronics over a period of six months with no known failures[28] provides clear evidence of the stability of "all-carbon" MJs.

Flexible and Transparent eC Junctions. Fabrication of stable electronic devices on a flexible substrate is a significant objective toward realizing next generation nanoelectronic technologies in consumer products.[68,69] As noted above, one disadvantage of PPF is the requirement for high pyrolysis temperatures over an ∼8 h period, which is impractical in commercial production, and especially for many flexible materials. The Au/eC substrate and eC/Au top contact can be applied at room temperature on a variety of substrates which would not tolerate PPF formation. Figure 6a shows images of complete Cr$_3$/Au$_{15}$/eC$_{10}$/AQ/eC$_{10}$/Au$_{15}$ MJs deposited on poly(ethylene terephthalate) (PET) "transparency" film, and
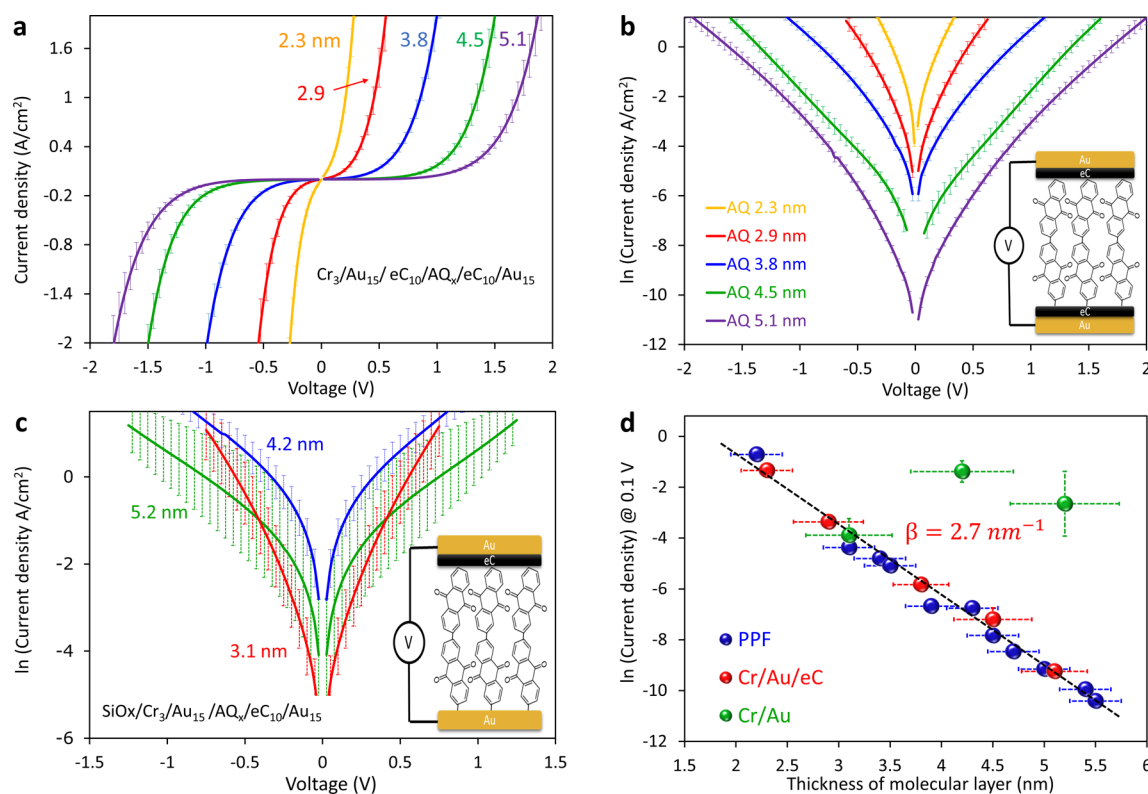
Figure 4. (a) Current density vs bias voltage (J−V) curves for junctions fabricated by Cr/Au/eC electrode as bottom contact, determined with a Keithley 2602A sourcemeter. AFM thicknesses of anthraquinone molecular layer are indicated in nanometers. Yield for tested junctions was 100% (nonshorted junctions) and error bars represent ±standard deviation for eight junctions of each thickness. (b) Semilogarithmic scale of J−V curves shown in panel (a). Right side inset: schematics of tested junctions (Cr layer under the Au is not shown in schematics). (c) Semilogarithmic scale of J−V curves for junctions fabricated by Cr/Au electrode as a bottom contact. Yield for tested junction was lower than 50% (nonshorted) and error bars represent ± standard deviation for nonshorted junctions. (d) Corresponding attenuation plot at 0.1 V for different bottom electrodes. β is the slope of observed for $SiO_x/Au_{15}/eC_{10}/AQ_x/eC_{10}/Au_{15}$ devices.
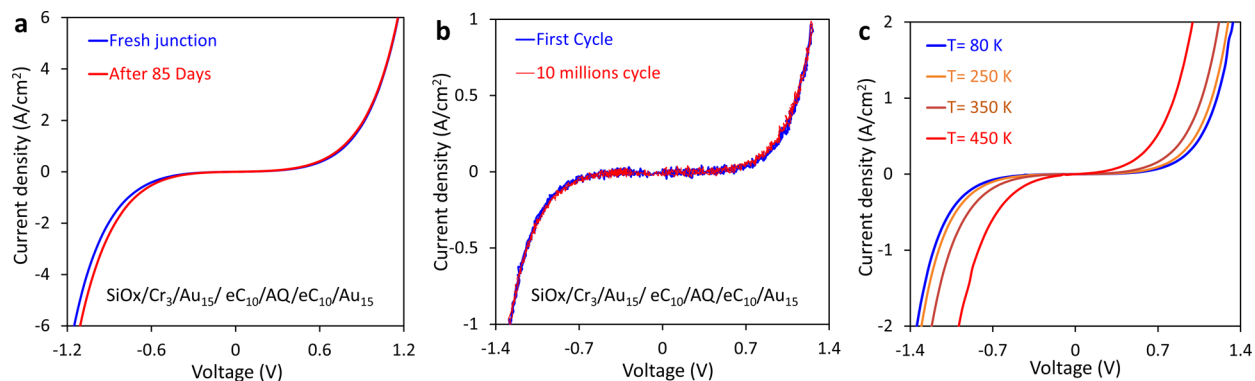
Figure 5. (a) Overlay of J−V curves for fresh Au/eC/AQ/eC/Au junction before and after being stored in ambient air for 85 days. AQ thickness ≈ 3.6 nm. (b) Overlay of J−V curve of a Au/eC/AQ/eC/Au junction before and after 10 million J−V cycles to ±1.3 V in air at 1000 V/sec. AQ thickness ≈ 4.4 nm. (c) J−V curves for a single Au/eC/AQ/eC/Au junction at four temperatures from 77 to 450 K in vacuum. AQ thickness ≈ 4.4 nm. Corresponding Arrhenius plot is shown in Supporting Information Figure S12. Junctions were deposited on a Si/SiO$_x$ substrate with 3 nm Cr adhesion layer in all cases.

Figure 6b shows the ability of the entire assembly to flex. Figure 6c (lines) is the J−V response for three different AQ thicknesses. Eight junctions for each thickness showed the same characteristic J−V shape as AQ devices on SiO$_x$ with no "shorts", however the standard deviation of J was higher. The variability was likely due to molecular layer thickness variations, possibly due to static charges which affected the electrochemical deposition. The points superimposed on the same curves are the J−V responses for each device after being flexed

100 times to the extent shown in Figure 6b. Because the total MJ thickness of ~60 nm is much less than the radius of curvature during bending, the strain on the MJ itself is small. In addition, eC is a disordered, amorphous type of carbon without crystalline structure which may make it more tolerant of mechanical stress in thin film structures.[42] Combined with strong bonding between eC and the molecular layer, the mechanical properties of eC provides stable junctions with identical J−V response before and after bending (Figure 6c).
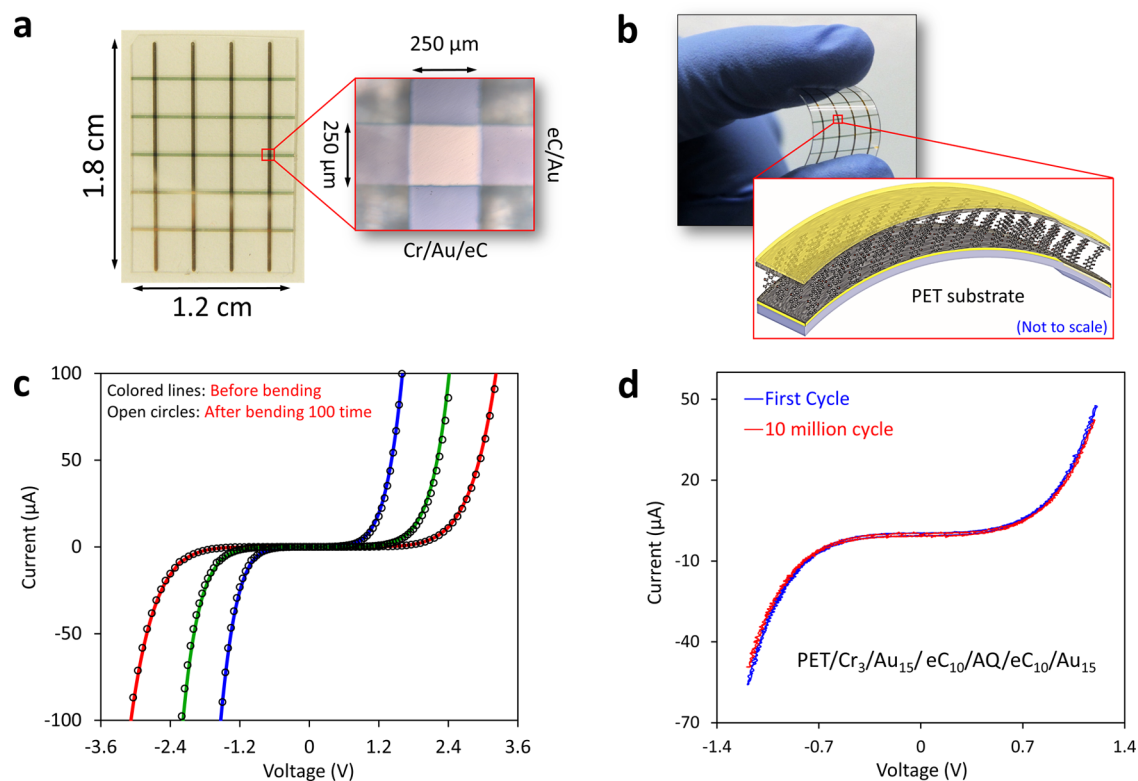
Figure 6. (a) Optical image of PET/Cr$_3$/Au$_{15}$/ eC$_{10}$/AQ/eC$_{10}$/Au$_{15}$ devices deposited on transparency film (PET). Magnification shows an individual junction. (b) Optical image of the fabricated device on PET substrate while bent. (c) $J-V$ curves of junctions fabricated on flexible PET substrate before (lines) and after (points) being bent 100 times to the degree shown in panel (b), which reduced the 1.8 cm dimension in panel (a) to ~1.4 cm. Three AQ thicknesses were deposited electrochemically but were not be verified by AFM. (d) Overlay of $J-V$ curve of freshly fabricated AQ junction on flexible PET substrate before (blue) and after (red) 10 million JV cycles to ± 1.3 V in air.

Note also that the PET surface is not flat on a nanometer scale like Si/SiO$_x$ or quartz substrate, but has defects visible in an optical microscope. Apparently, the MJ deposition process is sufficiently conformal, or the defects are sparse enough that yield is high, albeit with variations in current density. The PET substrate did not permit AFM "scratching"[70] to determine molecular layer thickness due to deformation and roughness, hence the thicknesses were estimated from the diazonium reduction conditions. Figure 6d shows the initial $J-V$ cycle for a PET/Cr/Au/eC/AQ/eC/Au device plus a second $J-V$ curve obtained after 10^7 bias cycles to ± 1.5 V, indicating excellent flexible device stability.

Molecular optoelectronics refers to an area that investigates both measurement capabilities (*e.g.*, optical spectroscopy) and our fundamental understanding of electronic transport mechanisms in molecular junctions.[71] Optoelectronics with molecular junctions requires one or both conducting contacts to be partially transparent in order to conduct measurements in the local environment. Both eC[31,32] and PPF[29,30] were investigated previously with the objective of making optically transparent carbon electrodes, usually on quartz substrates. However, the high sheet resistance of partially transparent layers of eC and PPF creates ohmic potential errors, which can be serious in either electrochemical or electronic applications. We have used metal/eC films previously for making sufficiently transparent top contacts on molecular junctions to monitor device structure while functioning with Raman[23,72] and UV−vis spectroscopy[73,74] and to observe light emission[20] by MJs. The combination of Au$_{15}$/eC$_{10}$ was used in the current work partly to provide transparency, and the combination of low sheet

resistance and optical transmission with the stability and surface chemistry of carbon makes Au/eC films attractive both as substrates and top contacts. Figure 7a shows absorbance spectra of several "blanket" e-beam coatings on a quartz slide, referenced to an uncoated slide in air. The Q/Cr$_3$/Au$_{15}$/eC$_{10}$ junction substrate, which is 30−40% transparent in the visible range, and the addition of anthraquinone layers (4−11 nm thick) yields additional absorbance in the region expected for free anthraquinone (220−280 nm). Figure 7b shows the same spectra after subtraction of the spectrum of an unmodified Q/Cr$_3$/Au$_{15}$/eC$_{10}$ sample, clearly showing the absorbance of the AQ layer. The Au$_{15}$/eC$_{10}$ electrode layer is clearly sufficiently transparent for optical spectroscopy and observation of photoeffects, including while the device is in operation, but to date such measurements have been constrained to reflection geometry through one partially transparent electrode. Figure 7c shows the absorbance of a complete molecular junction in *transmission* mode with the optical beam passing through both electrodes and the AQ layers. Subtraction of the spectrum of Q/Cr$_3$/Au$_{15}$/eC$_{20}$/Au$_{15}$ "blank" containing no AQ layer yields the spectra of Figure 7d. The spectra of Figure 7b and d are quite similar, with differences likely due to variation of internal reflection efficiencies at the AQ/eC interfaces. Although one transparent contact is sufficient for Raman monitoring of the device under bias in reflection geometry, the transmission geometry enabled by two transparent contacts is generally easier to interpret than reflection mode for UV−vis absorption spectroscopy.

Wafer Scale Lithography for eC Molecular Junctions. The Cr/Au/eC substrates shown in Figure 1 were deposited
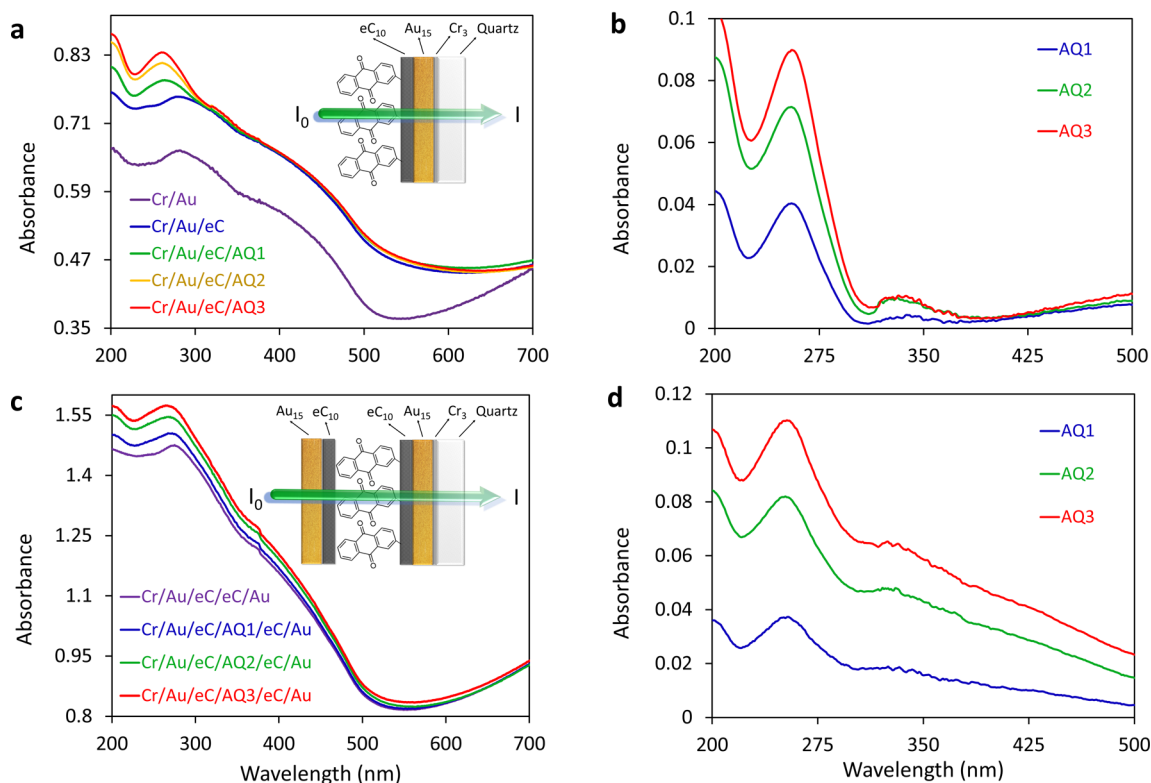
Figure 7. (a) Optical absorbance of Quartz/Cr$_3$/Au$_{15}$/eC$_{10}$/AQ relative to an air reference. Three different thicknesses of AQ molecular layer are shown. (b) Absorbance spectra of panel (a) following subtraction of the unmodified Q/Cr$_3$/Au$_{15}$/eC$_{10}$ spectrum, to yield the absorbance due to the AQ molecular layers. (c) Absorbance spectrum of complete Quartz/Cr$_3$/Au$_{15}$/eC$_{10}$/AQ/eC$_{10}$/Au$_{15}$ junction relative to an air reference, for three different thicknesses of Anthraquinone. (d) Absorbance from panel (c) following subtraction of the spectrum of a "blank" Q/Cr$_3$/Au$_{15}$/eC$_{20}$/Au$_{15}$ sample.
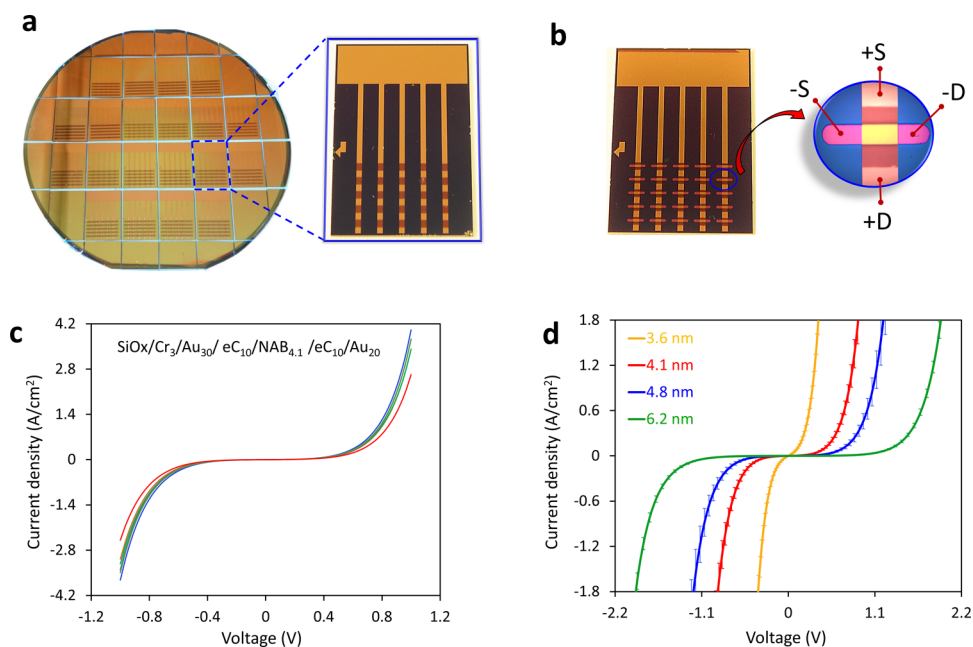
Figure 8. (a) Image and enlargement of 100 mm diameter wafer of integrated chip design after dicing but before molecular layer deposition. (b) Completed chip with 25 Si/SiO$_x$/Cr$_3$/Au$_{30}$/eC$_{10}$/NAB/eC$_{10}$/Au$_{20}$ after molecular layer and top contact deposition. NAB = nitroazobenzene oligomers. Magnification shows individual junction with the position of four probes for electrical contact to Au surfaces. (c) Overlay of J−V curves for 8 junctions selected randomly on a chip with a 4.1 nm thick layer of NAB. (d) Average J−V curves for integrated junctions with four different NAB thicknesses. Yield for tested junction was 100% of nonshorted junctions and error bars represent ±standard deviation for 6−8 junctions of each thickness. Statistics are provided in Supporting Information section 6.

through a shadow mask, which imposes constraints on the width and shapes of the "stripes" and the sharpness of their edges. Photolithography permits a wider range of patterns and dimensions, and a diced wafer consisting of 20 substrates made with conventional photolithography is shown in Figure 8a. When transparency is not required, the Au thickness was increased to 30 nm, so that the substrate pattern is initially Cr_3/Au_{30} across the entire chip. Contact with Au/eC with standard tungsten probes sometimes results in significant contact resistance in two-wire mode, so eC is deposited only on the junction region through a shadow mask. In the final junction shown in Figure 8b, the molecular layer is in contact only with eC at both electrodes, and the probes contact only Au, as shown. The Cr/Au/eC substrate may be coated with photoresist for protection during long-term storage or shipping, which is stripped off before modification with the molecular layer. The large Cr/Au pad at the top permits electrical contact to all five "stripes" during electrochemical reduction of the diazonium solution, and a razor cut after deposition across the five stripes isolates the electrode lines from each other for subsequent electronic testing. Finally, the eC/Au top contact is deposited on the modified Cr/Au/eC substrate through a shadow mask with a pattern of 25 rectangles, resulting in 25 MJs which can be contacted by 2, 3, or 4 probes on Au surfaces without stray currents or interference from nearby devices. We refer to the design of Figure 8b as "integrated", in order to distinguish it from the "crossbar" format of Figures 1 and 6 made entirely with shadow masks.

Four integrated MJ chips were used to make $Si/SiO_x/Cr_3/Au_{30}/eC_{10}/NAB_x/eC_{10}/Au_{20}$ molecular junctions, with the final resist layer of a chip shown in Figure 8a removed preceding electrochemical deposition of nitroazobenzene (NAB) molecular layer thicknesses of 3.6, 4.1, 4.8, and 6.2 nm. After deposition of the eC_{10}/Au_{20} top contacts, 28 MJs on the four samples were selected randomly and tested, involving 6−8 MJs on each chip. The yield was 100%, meaning that none of the devices exhibited an eC/eC short circuit. Figure 8c shows eight overlaid $J-V$ curves for the chip with NAB thickness of 4.1 nm, which had a relative standard deviation of current density of 13% for $|V| = 1$ V. Figure 8d shows averaged $J-V$ curves with error bars of ± standard deviation of J for the four thicknesses examined. Direct comparison of the $J-V$ responses for crossbar vs integrated MJs is difficult due to thickness differences, but the attenuation plots of $\ln J$ vs d may be compared directly. For the NAB MJs of the type shown in Figure 1, β (0.3 V) = 2.2 ± 0.31 nm^{-1} and an intercept of 6.3 ± 1.2, whereas the microfabricated devices had β (0.3 V) = 2.0 ± 0.22 nm^{-1} and an intercept of 5.7 ± 1.8. Therefore, the $J-V$ behavior of the integrated and crossbar eC/NAB/eC devices are statistically indistinguishable. Although the junctions shown in Figure 8b are relatively large (250 × 500 μm), eCarbon devices are completely compatible with previous lithographic methods[75] for fabricating a range of junction areas from 3 × 3 μm to 400 × 400 μm.

CONCLUSIONS

Successive e-beam deposition of carbon and Au provides the very flat surface, low sheet resistance, and chemical stability important to the fabrication and performance of molecular junctions. Au/eC as a substrate shows excellent behavior for surface modification by reduction of diazonium ions, and eC/molecule/eC have excellent lifetime and no apparent tendency to electromigration or oxidation. All-carbon MJs tolerate a

100−450 K temperature range and endure millions of $J-V$ cycles in ambient air without observable effects on electronic behavior. All-carbon MJs based on e-beam carbon may be deposited on flexible substrates and do not subject the substrate to high temperatures, thus significantly increasing the range of materials onto which molecular electronic devices can be incorporated. Partial transparency of one or both contact surfaces in all-carbon MJs permits live monitoring of molecular junctions under bias with optical spectroscopy as well as photocurrent generation and emission of photons. All three of these approaches have proven valuable as diagnostics of MJ structure and operation, and may have applications combining molecular electronics and photonics.

METHODS

The junction structure is shown in Figure 1, and is similar to the crossbar junctions reported previously using PPF substrates. The initial substrate was Si with 300 nm of SiO_x prepared by wet oxidation. Electron beam deposition was carried out in commercially available systems, either a Kurt Lesker PVD 75 or a Johnsen Ultravac 3000-GE vacuum system. A high energy (7 kV) electron beam is directed onto a target of Au or high purity graphite (source) by a magnetic field in a vacuum of 10^{-5} Torr or less. Atoms and clusters from the target then travel in a straight line to the sample, positioned normal to the atom beam and 20−30 cm from the e-beam target. In most cases, the electrode pattern was defined by a shadow mask with four parallel rectangular slots 250 μm wide. The work function of eC was determined with ultraviolet photoelectron spectroscopy[6] on four different samples with minimal air exposure to be 4.83 ± 0.06 eV, comparable to 4.7 ± 0.1 determined similarly for PPF. Electron-beam deposited carbon will be denoted as eC, and layer thicknesses by subscripts in nm, for example, Au_{15}/eC_{10}. Substrate layers of Cr, Au, and eC were deposited without breaking vacuum, as were the top contacts of eC/Au. The substrate Au layer was 15 nm in the crossbar geometry of Figure 1a in order to maximize transparency, but 20−30 nm layers yield similar results. In all cases the deposition rates were 0.03 nm/s for Cr, 0.03 nm/s for Au, and <0.01 nm/s for eC, with the e-beam current adjusted during eC deposition to keep the rate below 0.01 nm/sec. The target for eC deposition contained spectroscopically pure graphite rods (SPI Supplies, PA). The same deposition conditions were used to prepare Cr/Au/eC/molecule/eC/Au devices on PET transparency film, as described below. Detailed conditions for molecular layer deposition by diazonium ion reduction are similar to those reported previously,[6,38,75,76] and are listed in Supporting Information section 2.2. The anthraquinone layer is covalently bonded and partially ordered,[77,78] and thickness was always verified with AFM.[70] In all cases, the top contact was 10 nm of eC and 15 nm of Au, deposited by e-beam evaporation in one vacuum cycle.

In addition to the crossbar geometry of Figure 1, an "integrated" format shown in Figure 8 was fabricated with a lithographic lift-off process rather than shadow mask, in part to reduce contact resistance and also provide a wider range of junction dimensions. The full procedure is provided in Supporting Information section 6 and results in a "chip" of 25 molecular junctions, with the entire substrate protected by photoresist. The resist is removed by dimethyl sulfoxide (DMSO) before electrochemical reduction of the diazonium reagent to form the molecular layer. After deposition of the top contact through a shadow mask, the completed junctions have four Au pads for electrical contact.

Current−density vs bias voltage ($J-V$) curves were obtained in four-wire mode unless indicated otherwise, as described previously,[75] and UV−vis absorption spectra were obtained with a PerkinElmer Lambda 1050 dual beam spectrometer.

ASSOCIATED CONTENT

S Supporting Information

The Supporting Information is available free of charge on the ACS Publications website at DOI: 10.1021/acsnano.6b04900.

Additional details on fabrication, experimental conditions, statistics, and electrode characterization. (PDF)

AUTHOR INFORMATION

Corresponding Author
*E-mail: richard.mccreery@ualberta.ca.

Notes
The authors declare no competing financial interest.

ACKNOWLEDGMENTS

REFERENCES

(1) Metzger, R. M. Unimolecular Electronics. *Chem. Rev.* **2015**, *115*, 5056−5115.

(2) Xiang, D.; Wang, X.; Jia, C.; Lee, T.; Guo, X. Molecular-Scale Electronics: From Concept to Function. *Chem. Rev.* **2016**, *116*, 4318−4440.

(3) Amdursky, N.; Marchak, D.; Sepunaru, L.; Pecht, I.; Sheves, M.; Cahen, D. Electronic Transport via Proteins. *Adv. Mater.* **2014**, *26*, 7142−7161.

(4) Aviram, A.; Ratner, M. Molecular Rectifiers. *Chem. Phys. Lett.* **1974**, *29*, 277−283.

(5) Anariba, F.; Steach, J.; McCreery, R. Strong Effects of Molecular Structure on Electron Transport in Carbon/molecule/Copper Electronic Junctions. *J. Phys. Chem. B* **2005**, *109*, 11163−11172.

(6) Sayed, S. Y.; Fereiro, J. A.; Yan, H.; McCreery, R. L.; Bergren, A. J. Charge Transport in Molecular Electronic Junctions: Compression of the Molecular Tunnel Barrier in the Strong Coupling Regime. *Proc. Natl. Acad. Sci. U. S. A.* **2012**, *109*, 11498−11503.

(7) Baldea, I.; Xie, Z.; Frisbie, C. D. Uncovering A Law of Corresponding States for Electron Tunneling in Molecular Junctions. *Nanoscale* **2015**, *7*, 10465−10471.

(8) Choi, S. H.; Risko, C.; Delgado, M. C. R.; Kim, B.; Bredas, J.-L.; Frisbie, C. D. Transition from Tunneling to Hopping Transport in Long, Conjugated Oligo-imine Wires Connected to Metals. *J. Am. Chem. Soc.* **2010**, *132*, 4358−4368.

(9) Nijhuis, C. A.; Reus, W. F.; Whitesides, G. M. Mechanism of Rectification in Tunneling Junctions Based on Molecules with Asymmetric Potential Drops. *J. Am. Chem. Soc.* **2010**, *132*, 18386−18401.

(10) Nijhuis, C. A.; Reus, W. F.; Whitesides, G. M. Molecular Rectification in Metal-SAM-Metal Oxide-Metal Junctions. *J. Am. Chem. Soc.* **2009**, *131*, 17814−17827.

(11) Fluteau, T.; Bessis, C.; Barraud, C.; Della Rocca, M. L.; Martin, P.; Lacroix, J.-C.; Lafarge, P. Tuning the Thickness of Electrochemically Grafted Layers in Large Area Molecular Junctions. *J. Appl. Phys.* **2014**, *116*, 114509.

(12) Martin, P.; Della Rocca, M. L.; Anthore, A.; Lafarge, P.; Lacroix, J.-C. Organic Electrodes Based on Grafted Oligothiophene Units in Ultrathin, Large-Area Molecular Junctions. *J. Am. Chem. Soc.* **2012**, *134*, 154−157.

(13) Kim, T.; Liu, Z.-F.; Lee, C.; Neaton, J. B.; Venkataraman, L. Charge Transport and Rectification in Molecular Junctions Formed With Carbon-Based Electrodes. *Proc. Natl. Acad. Sci. U. S. A.* **2014**, *111*, 10928−10932.

(14) Hong, J.-Y.; Jeon, S. O.; Jang, J.; Song, K.; Kim, S. H. A Facile Route For The Preparation Of Organic Bistable Memory Devices Based On Size-Controlled Conducting Polypyrrole Nanoparticles. *Org. Electron.* **2013**, *14*, 979−983.

(15) Wu, J.; McCreery, R. L. Solid-State Electrochemistry in Molecule/TiO2Molecular Heterojunctions as the Basis of the TiO2 ″Memristor″. *J. Electrochem. Soc.* **2009**, *156*, P29−P37.

(16) Galperin, M.; Nitzan, A. Molecular Optoelectronics: the Interaction of Molecular Conduction Junctions With Light. *Phys. Chem. Chem. Phys.* **2012**, *14*, 9421−9438.

(17) Fereiro, J. A.; Kondratenko, M.; Bergren, A. J.; McCreery, R. L. Internal Photoemission in Molecular Junctions: Parameters for Interfacial Barrier Determinations. *J. Am. Chem. Soc.* **2015**, *137*, 1296−1304.

(18) Banerjee, P.; Conklin, D.; Nanayakkara, S.; Park, T.-H. H.; Therien, M. J.; Bonnell, D. A. Plasmon-Induced Electrical Conduction In Molecular Devices. *ACS Nano* **2010**, *4*, 1019−1025.

(19) Conklin, D.; Nanayakkara, S.; Park, T. H.; Lagadec, M. F.; Stecher, J. T.; Chen, X.; Therien, M. J.; Bonnell, D. Exploiting Plasmon-Induced Hot Electrons in Molecular Electronic Devices. *ACS Nano* **2013**, *7*, 4479−4486.

(20) Ivashenko, O.; Bergren, A. J.; McCreery, R. L. Light Emission as a Probe of Energy Losses in Molecular Junctions. *J. Am. Chem. Soc.* **2016**, *138*, 722−725.

(21) Du, W.; Wang, T.; Chu, H.-S.; Wu, L.; Liu, R.; Sun, S.; Phua, W. K.; Wang, L.; Tomczak, N.; Nijhuis, C. A. On-chip molecular electronic plasmon sources based on self-assembled monolayer tunnel junctions. *Nat. Photonics* **2016**, *10*, 274−280.

(22) Marquardt, C. W.; Grunder, S.; Błaszczyk, A.; Dehm, S.; Hennrich, F.; Löhneysen, H. V.; Mayor, M.; Krupke, R. Electroluminescence From a Single Nanotube-Molecule-Nanotube Junction. *Nat. Nanotechnol.* **2010**, *5*, 863−867.

(23) Kumar, R.; Pillai, R. G.; Pekas, N.; Wu, Y.; McCreery, R. L. Spatially Resolved Raman Spectroelectrochemistry of Solid-State Polythiophene/Viologen Memory Devices. *J. Am. Chem. Soc.* **2012**, *134*, 14869−14876.

(24) Lacaze, P. C.; Lacroix, J.-C. *Non-Volatile Memories*; ISTE Ltd.: London, U.K., 2014.

(25) Migliore, A.; Nitzan, A. Nonlinear Charge Transport in Redox Molecular Junctions: A Marcus Perspective. *ACS Nano* **2011**, *5*, 6669−6685.

(26) Bergren, A. J.; McCreery, R. L.; Stoyanov, S. R.; Gusarov, S.; Kovalenko, A. Electronic Characteristics and Charge Transport Mechanisms for Large Area Aromatic Molecular Junctions. *J. Phys. Chem. C* **2010**, *114*, 15806−15815.

(27) Mahmoud, A. M.; Bergren, A. J.; Pekas, N.; McCreery, R. L. Towards Integrated Molecular Electronic Devices: Characterization of Molecular Layer Integrity During Fabrication Processes. *Adv. Funct. Mater.* **2011**, *21*, 2273−2281.

(28) Bergren, A. J.; Zeer-Wanklyn, L.; Semple, M.; Pekas, N.; Szeto, B.; McCreery, R. L. Musical Molecules: the Molecular Junction as an Active Component in Audio Distortion Circuits. *J. Phys.: Condens. Matter* **2016**, *28*, 094011.

(29) Donner, S.; Li, H. W.; Yeung, E. S.; Porter, M. D. Fabrication of Optically Transparent Carbon Electrodes by the Pyrolysis of Photoresist Films: Approach to Single-Molecule Spectroelectrochemistry. *Anal. Chem.* **2006**, *78*, 2816−2822.

(30) Tian, H.; Bergren, A. J.; McCreery, R. L. UltravioletVisible Spectroelectrochemistry of Chemisorbed Molecular Layers on Optically Transparent Carbon Electrodes. *Appl. Spectrosc.* **2007**, *61*, 1246−1253.

(31) Mattson, J. S.; Smith, C. A. Optically Transparent Carbon Film Electrodes for Infrared Spectroelectrochemistry. *Anal. Chem.* **1975**, *47*, 1122−1125.

(32) DeAngelis, T. P.; Hurst, R. W.; Yacynych, A. M.; Mark, H. B., Jr.; Heineman, W. R.; Mattson, J. S. Carbon and Mercury-Carbon Optically Transparent Electrodes. *Anal. Chem.* **1977**, *49*, 1395−1398.

(33) Blackstock, J. J.; Rostami, A. A.; Nowak, A. M.; McCreery, R. L.; Freeman, M.; McDermott, M. T. Ultraflat Carbon Film Electrodes Prepared by Electron Beam Evaporation. *Anal. Chem.* **2004**, *76*, 2544−2552.

(34) Conley, J. F., Jr; Alimardani, N. *Rectenna Solar Cells*; Springer Science: New York, 2013; pp 111−134.

(35) Cowell, E. W.; Alimardani, N.; Knutson, C. C.; Conley, J. F.; Keszler, D. A.; Gibbons, B. J.; Wager, J. F. Advancing MIM Electronics: Amorphous Metal Electrodes. *Adv. Mater.* **2011**, *23*, 74−78.

(36) Yang, S.; Kymissis, I.; Leland, E. S.; Liu, S.; O'Brien, S. Influence of electromigration on the maximum operating field of (Ba,Sr)TiO3/parylene-C composite capacitors. *J. Vac. Sci. Technol., B: Microelectron. Nanometer Struct.* **2013**, *31*, 060603.

(37) Ranganathan, S.; McCreery, R. L. Electroanalytical Performance of Carbon Films with Near-Atomic Flatness. *Anal. Chem.* **2001**, *73*, 893−900.

(38) Yan, H.; Bergren, A. J.; McCreery, R. L. All-Carbon Molecular Tunnel Junctions. *J. Am. Chem. Soc.* **2011**, *133*, 19168−19177.

(39) Ranganathan, S.; McCreery, R. L.; Majji, S. M.; Madou, M. Photoresist-Derived Carbon for Microelectrochemical Applications. *J. Electrochem. Soc.* **2000**, *147*, 277−282.

(40) Fairman, C.; Yu, S.; Liu, G.; Downard, A.; Hibbert, D.; Gooding, J. Exploration of Variables in the Fabrication of Pyrolysed Photoresist. *J. Solid State Electrochem.* **2008**, *12*, 1357−1365.

(41) Yu, S. S. C.; Downard, A. J. Photochemical Grafting and Activation of Organic Layers on Glassy Carbon and Pyrolyzed Photoresist Films. *Langmuir* **2007**, *23*, 4662−4668.

(42) Robertson, J. Diamond-Like Amorphous Carbon. *Mater. Sci. Eng., R* **2002**, *37*, 129−281.

(43) Ferrari, A. C.; Robertson, J. Interpretation of Raman Spectra of Disordered and Amorphous Carbon. *Phys. Rev. B: Condens. Matter Mater. Phys.* **2000**, *61*, 14095−14107.

(44) Jackson, S. T.; Nuzzo, R. G. Determining Hybridization Differences for Amorphous Carbon From the XPS C 1s Envelope. *Appl. Surf. Sci.* **1995**, *90*, 195−203.

(45) Jia, J.; Kato, D.; Kurita, R.; Sato, Y.; Maruyama, K.; Suzuki, K.; Hirono, S.; Ando, T.; Niwa, O. Structure and Electrochemical Properties of Carbon Films Prepared by a Electron Cyclotron Resonance Sputtering Method. *Anal. Chem.* **2007**, *79*, 98−105.

(46) Wang, S.; Swain, G. M. Spatially Heterogeneous Electrical and Electrochemical Properties of Hydrogen-Terminated Boron-Doped Nanocrystalline Diamond Thin Film Deposited from an Argon-Rich CH4/H2/Ar/B2H6 Source Gas Mixture. *J. Phys. Chem. C* **2007**, *111*, 3986−3995.

(47) Stotter, J.; Show, Y.; Wang, S.; Swain, G. Comparison of the Electrical, Optical, and Electrochemical Properties of Diamond and Indium Tin Oxide Thin-Film Electrodes. *Chem. Mater.* **2005**, *17*, 4880−4888.

(48) Swain, G. M. Electrically Conducting Diamond Thin Films: Advanced Electrode Materials for Electrochemical Technologies. In *Electroanalytical Chemistry*; Bard, A. J., Rubinstein, I., Eds.; Dekker: New York, 2004; Vol. 22, pp 181−277.

(49) Pleskov, Y.; Krotova, M.; Ralchenko, V.; Saveliev, A.; Bozhko, A. Electrochemical behavior of nitrogenated nanocrystalline diamond electrodes. *Russ. J. Electrochem.* **2007**, *43*, 827.

(50) Yang, N.; Uetsuka, H.; Osawa, E.; Nebel, C. E. Vertically Aligned Nanowires from Boron-Doped Diamond. *Nano Lett.* **2008**, *8*, 3572−3576.

(51) Kamata, T.; Kato, D.; Ida, H.; Niwa, O. Structure and Electrochemical Characterization of Carbon Films Formed by Unbalanced Magnetron (ubm) Sputtering Method. *Diamond Relat. Mater.* **2014**, *49*, 25−32.

(52) Sekioka, N.; Kato, D.; Ueda, A.; Kamata, T.; Kurita, R.; Umemura, S.; Hirono, S.; Niwa, O. Controllable Electrode Activities of Nano-Carbon Films While Maintaining Surface Flatness by Electrochemical Pretreatment. *Carbon* **2008**, *46*, 1918−1926.

(53) Rabache, V.; Chaste, J.; Petit, P.; Della Rocca, M. L.; Martin, P.; Lacroix, J.-C.; McCreery, R. L.; Lafarge, P. Direct Observation of Large Quantum Interference Effect in Anthraquinone Solid-State Junctions. *J. Am. Chem. Soc.* **2013**, *135*, 10218−10221.

(54) Wan, A.; Jiang, L.; Sangeeth, C. S. S.; Nijhuis, C. A. Reversible Soft Top-Contacts to Yield Molecular Junctions with Precise and Reproducible Electrical Characteristics. *Adv. Funct. Mater.* **2014**, *24*, 4442−4456.

(55) Nijhuis, C. A.; Reus, W. F.; Siegel, A. C.; Whitesides, G. M. A Molecular Half-Wave Rectifier. *J. Am. Chem. Soc.* **2011**, *133*, 15397−15411.

(56) Smith, C. E.; Odoh, S. O.; Ghosh, S.; Gagliardi, L.; Cramer, C. J.; Frisbie, C. D. Length-Dependent Nanotransport and Charge Hopping Bottlenecks in Long Thiophene-Containing π-Conjugated Molecular Wires. *J. Am. Chem. Soc.* **2015**, *137*, 15732−15741.

(57) Luo, L.; Choi, S. H.; Frisbie, C. D. Probing Hopping Conduction in Conjugated Molecular Wires Connected to Metal Electrodes. *Chem. Mater.* **2011**, *23*, 631−645.

(58) Cademartiri, L.; Thuo, M. M.; Nijhuis, C. A.; Reus, W. F.; Tricard, S.; Barber, J. R.; Sodhi, R. N. S.; Brodersen, P.; Kim, C.; Chiechi, R. C.; Whitesides, G. M. Electrical Resistance of AgTS−S(CH2)n−1CH3//Ga2O3/EGaIn Tunneling Junctions. *J. Phys. Chem. C* **2012**, *116*, 10848−10860.

(59) Dickey, M. D.; Chiechi, R. C.; Larsen, R. J.; Weiss, E. A.; Weitz, D. A.; Whitesides, G. M. Eutectic Gallium-Indium (EGaIn): A Liquid Metal Alloy for the Formation of Stable Structures in Microchannels at Room Temperature. *Adv. Funct. Mater.* **2008**, *18*, 1097−1104.

(60) Beebe, J. M.; Kim, B.; Frisbie, C. D.; Kushmerick, J. G. Measuring Relative Barrier Heights in Molecular Electronic Junctions with Transition Voltage Spectroscopy. *ACS Nano* **2008**, *2*, 827−832.

(61) Taherinia, D.; Smith, C. E.; Ghosh, S.; Odoh, S. O.; Balhorn, L.; Gagliardi, L.; Cramer, C. J.; Frisbie, C. D. Charge Transport in 4 nm Molecular Wires with Interrupted Conjugation: Combined Experimental and Computational Evidence for Thermally Assisted Polaron Tunneling. *ACS Nano* **2016**, *10*, 4372−4383.

(62) McCreery, R.; Yan, H.; Bergren, A. J. A Critical Perspective on Molecular Electronic Junctions: There is Plenty of Room in the Middle. *Phys. Chem. Chem. Phys.* **2013**, *15*, 1065−1081.

(63) Song, P.; Sangeeth, C. S. S.; Thompson, D.; Du, W.; Loh, K. P.; Nijhuis, C. A. Noncovalent Self-Assembled Monolayers on Graphene as a Highly Stable Platform for Molecular Tunnel Junctions. *Adv. Mater.* **2016**, *28*, 631−639.

(64) Seo, S.; Min, M.; Lee, S. M.; Lee, H. Photo-Switchable Molecular Monolayer Anchored Between Highly Transparent And Flexible Graphene Electrodes. *Nat. Commun.* **2013**, *4*, 1920.

(65) Wang, G.; Kim, Y.; Choe, M.; Kim, T.-W. W.; Lee, T. A New Approach For Molecular Electronic Junctions With a Multilayer Graphene Electrode. *Adv. Mater.* **2011**, *23*, 755−760.

(66) Kim, D.; Jeong, H.; Lee, H.; Hwang, W.-T. T.; Wolf, J.; Scheer, E.; Huhn, T.; Jeong, H.; Lee, T. Flexible Molecular-Scale Electronic Devices Composed Of Diarylethene Photoswitching Molecules. *Adv. Mater.* **2014**, *26*, 3968−3973.

(67) Akkerman, H. B.; Blom, P. W. M.; de Leeuw, D. M.; de Boer, B. Towards Molecular Electronics With Large-Area Molecular Junctions. *Nature* **2006**, *441*, 69.

(68) Akinwande, D.; Petrone, N.; Hone, J. Two-Dimensional Flexible Nanoelectronics. *Nat. Commun.* **2014**, *5*, 5678.

(69) Cheng, T.; Zhang, Y.; Lai, W.-Y.; Huang, W. Stretchable Thin-Film Electrodes for Flexible Electronics with High Deformability and Stretchability. *Adv. Mater.* **2015**, *27*, 3349−3376.

(70) Anariba, F.; DuVall, S. H.; McCreery, R. L. Mono- and Multilayer Formation by Diazonium Reduction on Carbon Surfaces Monitored with Atomic Force Microscopy "Scratching". *Anal. Chem.* **2003**, *75*, 3837−3844.

(71) Aradhya, S. V.; Venkataraman, L. Single-molecule junctions beyond electronic transport. *Nat. Nanotechnol.* **2013**, *8*, 399−410.

(72) Nowak, A. M.; McCreery, R. L. *In Situ* Raman Spectroscopy of Bias-Induced Structural Changes in Nitroazobenzene Molecular Electronic Junctions. *J. Am. Chem. Soc.* **2004**, *126*, 16621−16631.

(73) Bonifas, A. P.; McCreery, R. L. Solid State Spectroelectrochemistry of Redox Reactions in Polypyrrole/Oxide Molecular Heterojunctions. *Anal. Chem.* **2012**, *84*, 2459−2465.

(74) Bonifas, A. P.; McCreery, R. L. *In-Situ* Optical Absorbance Spectroscopy of Molecular Layers in Carbon Based Molecular Electronic Devices. *Chem. Mater.* **2008**, *20*, 3849−3856.

(75) Ru, J.; Szeto, B.; Bonifas, A.; McCreery, R. L. Microfabrication and Integration of Diazonium-Based Aromatic Molecular Junctions. *ACS Appl. Mater. Interfaces* **2010**, *2*, 3693−3701.

(76) McCreery, R.; Wu, J.; Kalakodimi, R. J. Electron Transport and Redox Reactions in Carbon Based Molecular Electronic Junctions. *Phys. Chem. Chem. Phys.* **2006**, *8*, 2572−2590.

(77) Chernyy, S.; Bousquet, A.; Torbensen, K.; Iruthayaraj, J.; Ceccato, M.; Pedersen, S. U.; Daasbjerg, K. Elucidation of the Mechanism of Redox Grafting of Diazotated Anthraquinone. *Langmuir* **2012**, *28*, 9573−9582.

(78) Bousquet, A.; Ceccato, M.; Hinge, M.; Pedersen, S. U.; Daasbjerg, K. Redox Grafting of Diazotated Anthraquinone as a Means of Forming Thick Conducting Organic Films. *Langmuir* **2012**, *28*, 1267−1275.